Temperature- and thickness-dependence of robust out-of-plane ferroelectricity in CVD grown ultrathin van der Waals α-In layers

Weng Fu Io[1], Shuoguo Yuan[1], Sin Yi Pang[1], Lok Wing Wong[1], Jiong Zhao[1], Jianhua Hao[1]*

1 Department of Applied Physics, The Hong Kong Polytechnic University,
Hong Kong, P. R. China.

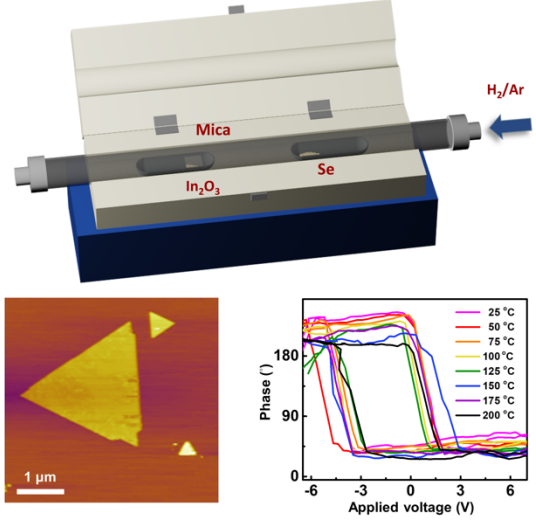

CVD grown 2D α-In layers own robust and intrinsic out-of-plane ferroelectricity maintained at high-temperature.

Io, W. F., Yuan, S., Pang, S. Y., Wong, L. W., Zhao, J., & Hao, J. (2020). Temperature-and thickness-dependence of robust out-of-plane ferroelectricity in CVD grown ultrathin van der Waals α-In 2 Se 3 layers. Nano research, 13, 1897-1902.

Temperature- and thickness-dependence of robust out-of-plane ferroelectricity in CVD grown ultrathin van der Waals α-In_2Se_3 layers

Weng Fu Io[1], Shuoguo Yuan[1], Sin Yi Pang[1], Lok Wing Wong[1], Jiong Zhao[1], Jianhua Hao[1]

[1] *Department of Applied Physics, The Hong Kong Polytechnic University, Hong Kong, P. R. China.*

ABSTRACT

Two-dimensional (2D) ferroelectric materials with unique structure and extraordinary optoelectrical properties have attracted intensive research in the field of nanoelectronic and optoelectronic devices, such as optical sensors, transistors, photovoltaics and non-volatile memory devices. However, the transition temperature of the reported ferroelectrics in 2D limit is generally low or slightly above room temperature, hampering their applications in high-temperature electronic devices. Here, we report the robust high-temperature ferroelectricity in 2D α-In_2Se_3, grown by chemical vapor deposition (CVD), exhibiting an out-of-plane spontaneous polarization reaching above 200 °C. The polarization switching and ferroelectric domains are observed in In_2Se_3 nanoflakes in a wide temperature range. The coercive field of the CVD grown ferroelectric layers illustrates a room-temperature thickness dependency and increases drastically when the film thickness decreases; whereas there is no large variance in the coercive field at different temperature from the samples with identical thickness. The results show the stable ferroelectricity of In_2Se_3 nanoflakes maintained at high temperature and open up the opportunities of 2D materials for novel applications in high-temperature nanoelectronic devices.

KEYWORDS

In_2Se_3, 2D materials, ferroelectricity, high-temperature, coercive field

1. Introduction

Ferroelectric materials have been extensively used for practical device applications in the past decades. The pursuance for high density and capacity devices for future technological development has intensively promoted the research on reducing both the vertical and lateral size of the ferroelectrics. Two-dimensional (2D) ferroelectric materials, which have attracted considerable attentions owing to their superior electrical, optical and pyroelectric properties, are highly desirable for the future nanoelectronic applications [1-6]. However, the ferroelectricity of the traditional ferroelectric materials deteriorates when their thickness approaches to the 2D limit, and eventually vanishes at a critical thickness [7-9]. Moreover, the phase transition temperature, i.e. Curie temperature T_c and the polarization strength of those ferroelectrics inevitably decline with the reduction in thickness, further restricting the size miniaturization of the conventional ferroelectric devices and their potential applications in high-temperature electronic devices [10, 11]. The suppression of spontaneous polarization in the ferroelectrics when scaled down results from the internal depolarization field generated by accumulated charges at the ferroelectric interfaces and not completely be compensated [1,7].

To date, several 2D van der Waals (vdW) materials are reported to retain ferroelectricity in atomically thin thickness, which are promising to address the fundamental size limit issue of the traditional ferroelectrics. Monolayer SnTe and group-IV monochalcogenides are experimentally demonstrated with the existence of in-plane (IP) ferroelectricity [12,13]. Nonetheless, the Curie temperature T_c of monolayer SnTe is below room-temperature, and the IP polarization direction largely limiting its potential for practical applications due to the complicated circuit designs [12]. Besides, room-temperature out-of-plane (OOP) ferroelectricity was experimentally observed in a few 2D vdW materials such as $CuInP_2S_6$, $MoTe_2$, WTe_2 and α-In_2Se_3 [14-17]. In particular, α-In_2Se_3 exhibits two distinct stacking arrangements, known as the hexagonal (2H) and rhombohedral (3R) structures. Both structures are theoretically and experimentally evident with the existence of intercorrelated IP and OOP ferroelectricity [18-24], distinguishing the In_2Se_3 from other currently reported 2D vdW ferroelectric materials. Various electronic structures based on 2D α-In_2Se_3 are fabricated including ferroresistive Schottky diodes and ferroelectric field-effect transistors, enabling diverse functionalities as optoelectronics and non-volatile memory, and utilizing the IP and OOP ferroelectricity of the material [18-20, 23-25]. In a stark contrast to other 2D vdW ferroelectrics, In_2Se_3 enjoys a Curie temperature much higher than room temperature. High transition temperature of structure variation up to ~427 ºC is observed in a four-layer α-In_2Se_3 through measurement of second harmonic generation spectroscopy [22]. Nevertheless, as an emerging 2D vdW ferroelectric material, the ferroelectric characteristics of In_2Se_3 at higher temperature are not explored yet, which are essential for high-temperature device applications. Herein, we report the observation of intrinsic OOP ferroelectricity from room-temperature to 200 ºC in α-In_2Se_3 nanosheets synthesized by chemical vapor deposition (CVD). The as-grown α-In_2Se_3 samples are beneficial for large-scale fabrication with uniform lateral dimension, good crystallinity and high controllability. In ferroelectrics, the polarization direction can be reversed by external electric bias, known as the coercive field (E_c). By using piezoresponse force microscopy (PFM), the room-temperature

Address correspondence to jh.hao@polyu.edu.hk

OOP ferroelectric polarization and the thickness-dependence of coercive field of α-In_2Se_3 were characterized. Additionally, temperature-varied polarity switching and coercive field behaviors of α-In_2Se_3 were primarily examined. Our work reveals the great feasibility of 2D α-In_2Se_3 films in high-temperature electronic applications.

2. Results and discussion

2.1 Characterization of CVD-grown α-In_2Se_3

High-quality 2D In_2Se_3 thin films were synthesized via CVD technique, and the schematic diagram of the fabrication system and the atomic structure of the as-grown non-centrosymmetric 3R In_2Se_3 on mica substrate are shown in Fig. 1(a) and 1(b), respectively [26]. In α-In_2Se_3 layer structure, there are five atomic layers (Se−In−Se−In−Se) stacking in the z-direction and each In_2Se_3 layer is bonded through weak vdW interactions. The OOP ferroelectricity originates from off-centering Se atom in the middle of the quintuple layers of α-In_2Se_3. Figure 2(a) demonstrates the optical image of triangular In_2Se_3 thin films grown on mica substrates with lateral size of ~10 μm. As presented in Fig. 2(b), the AFM image and height profile show that 3 nm In_2Se_3 corresponding to 3 layers was grown with notably sharp edges and uniform surface, indicating a good crystalline quality. Raman spectroscopy and X-ray photoelectron spectroscopy (XPS) were performed to identify and inspect the crystal quality of the as-synthesized In_2Se_3. Figure 2(c) illustrates the Raman spectrum of the In_2Se_3 samples, and three peaks are identified at ~107, 170 and 203 cm^{-1} attributing to A_1 (LO+TO), A_1(TO) and A_1 (LO) phonon modes of α-phase In_2Se_3, respectively. The measured results are in agreement with the reported values [18-19]. The Raman mapping result as shown in Fig. 2(d) was obtained by plotting the Raman intensity at 107 cm^{-1}, corresponding to the A_1 (LO+TO) phonon mode of α-In_2Se_3 under 532 nm laser excitation at 0.3 mW, verifying the pure α-phase of the In_2Se_3 nanoflake. XPS was subsequently carried out to analyze the elemental composition of the CVD-grown α-In_2Se_3 and the spectra are displayed in Fig. 2(e). The strong XPS doublets at 444.9 and 452.6 eV are assigned to the

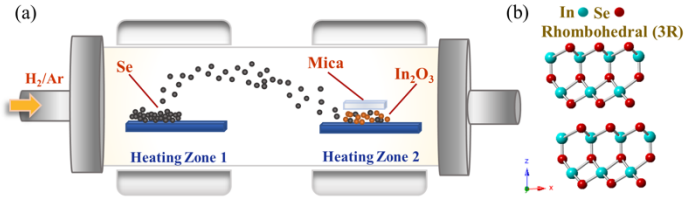

Figure 1 CVD system for In_2Se_3 growth. (a) Schematic diagram of the CVD growth process of ultrathin In_2Se_3 on mica substrates. (b) Schematic of crystal structure of In_2Se_3 (red: Se atoms and blue: In atoms).

In $3d_{5/2}$ and In $3d_{3/2}$ core level orbitals, respectively, and the pair of peaks at 54.2 and 54.7 eV are responsible for Se $3d_{5/2}$, Se $3d_{3/2}$ orbitals respectively, validating the chemical composition of the as-grown nanosheets. In addition, Fig. 2(f) demonstrates the high-resolution transmission electron microscopy (HRTEM) image of the top-view α-In_2Se_3, showing a periodic and uniform hexagonal crystal lattice with lattice spacing of ~0.36 nm, and the selected area electron diffraction (SAED) pattern in the inset presents a 6-fold symmetry, both suggesting a high crystallinity of the synthesized samples. The above characterizations indicate the successful fabrication of single-crystalline α-In_2Se_3 nanoflakes.

2.2 Room-temperature ferroelectric measurements

It is known that PFM is an effective technique to illustrate the presence of spontaneous and switchable polarization in nanoscale samples. Therefore, it is employed to study the ferroelectric characteristics of the 2D α-In_2Se_3 in the following measurements. For all the PFM investigations, the α-In_2Se_3 samples were transferred onto conductive Pt substrates. The PFM phase and amplitude signals are able to manifest the polarization direction and local piezoelectric response of measured samples. Figure 3(a) displays the topography image of an 8 nm triangular α-In_2Se_3 nanosheet which was cracked during the water-assisted transfer process from mica to Pt substrate, and the height profile is shown in Fig. S1 in the Electronic Supplementary Material (ESM). There is obvious phase contrast difference in the OOP direction (Fig. 3(b)) and single ferroelectric domain can be clearly visualized in the α-In_2Se_3 triangle. Reversal of the polarity state by external electric field is one of the key features for ferroelectric materials. Figure 3(c) illustrates the OOP PFM phase and amplitude hysteresis loops of the corresponding 8 nm α-In_2Se_3 scanned by dc triangular waveform from -8 V to 8 V. The off-field phase hysteresis loop clearly shows two discrete polarization states with ~180° phase difference and asymmetric butterfly loop is observed in the amplitude signal. The difference between two minima of the amplitude signal is ~3.75 V, which is consistent with the switching voltage of the ferroelectric polarization. Furthermore, PFM phase

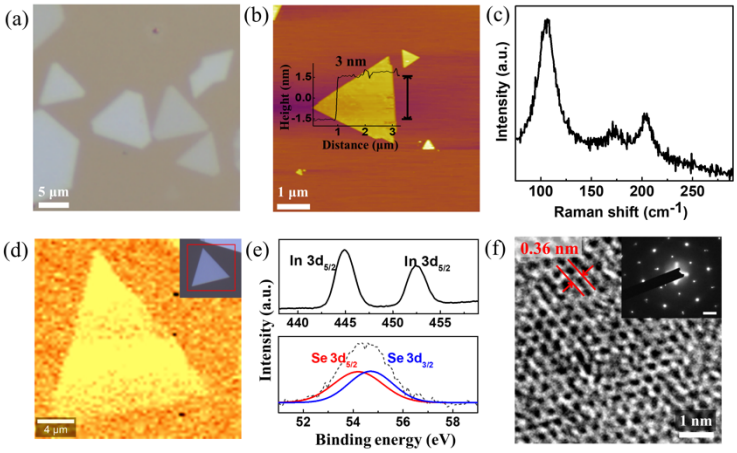

Figure 2 Structural characterization of the as-grown In_2Se_3. (a) Optical image of triangular In_2Se_3 grown on mica. (b) AFM image and the corresponding height profile of In_2Se_3 with the thickness of ~3 nm. (c) Raman spectrum and (d) Raman mapping of In_2Se_3 on mica, with excitation laser wavelength of 532 nm. Inset: optical image of the mapped area. (e) XPS spectra of In 3d and Se 3d core levels of In_2Se_3 nanosheets. (f) HRTEM image of In_2Se_3 thin film, inset is the corresponding SAED pattern and the inset scale bar is 2 1/nm.

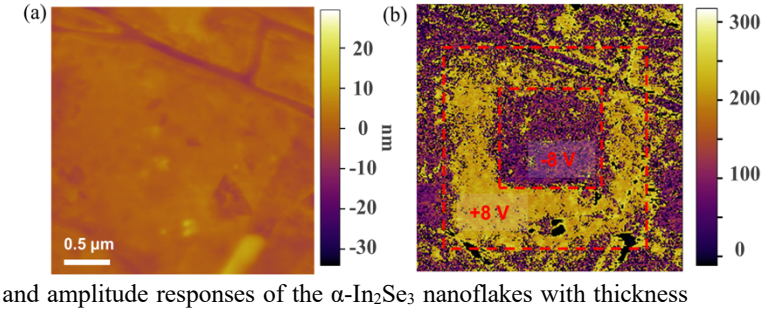

and amplitude responses of the α-In_2Se_3 nanoflakes with thickness

of 11 nm, 20 nm, 25 nm, 55 nm, and 62 nm were also acquired (Fig. 3(d)-(h)), and obvious 180° phase switching and butterfly-shaped amplitude behaviors are identified. To further verify the accuracy of the ferroelectric behaviors, the measurements were repeated for several times at different selected regions of the same nanosheet and nearly identical responses were obtained, associated with small variance. These results indicate that 2D CVD-grown α-In_2Se_3 possesses a stable room-temperature ferroelectric polarization of the layers at different thickness.

The coercive field of ferroelectric materials provides important information for device designs in technological aspect, as the majority of novel electronic devices are demanding for a low operating voltage for less power consumption. In the devices cooperated with ferroelectrics, the operating voltages are usually greater than their coercive voltage. Therefore, the characterization of the coercive field for flipping the polarization direction is engaging a high interest. By taking the average of multiple measurements of the PFM hysteresis loops, the values of the coercive field were obtained and then plotted as a function of the layer thickness (Fig. 3(i)). From 62 nm to 8 nm thick α-In_2Se_3, the E_c for polarization switching at room-temperature rises from ~0.054 V/nm to ~0.33 V/nm. The E_c and film thickness are non-linearly related, where the value of E_c increases rapidly below ~25 nm. When the α-In_2Se_3 films become thicker, the E_c gradually drops due to weakened effect of the depolarization field, resembling the trend discovered in other typical ferroelectrics [27-29].

Moreover, the ferroelectric switching characteristics of α-In_2Se_3 were examined by controlling the domain pattern of ultrathin α-In_2Se_3 films. For sample's preparation, α-In_2Se_3 nanoflakes were mechanically exfoliated onto Pt substrate. Figure 4(a) and (b) demonstrate the topography and OOP phase images of a 6 nm α-In_2Se_3 film collected after writing two square patterns with opposite tip voltages (+8V and -8 V). The discernible modified domain pattern illustrates that polarization direction of the α-In_2Se_3 can be reversed by the external bias, thus providing a solid evidence for the presence of intrinsic ferroelectricity in 2D α-In_2Se_3.

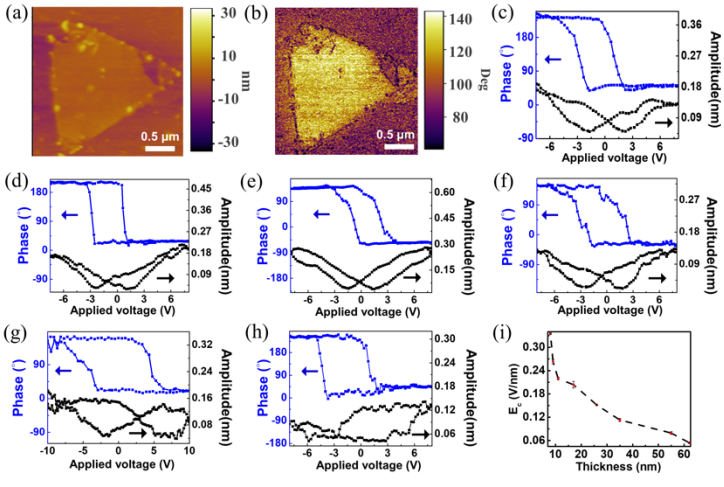

Figure 3 Ferroelectric properties of the CVD-grown In_2Se_3 transferred onto Pt/ substrate. (a) AFM topographic image and (b) corresponding PFM OOP phase image of an 8 nm In_2Se_3 nanoflake. (c-h) Local ferroelectric hysteresis loops of 8 nm, 11nm 20 nm, 25 nm, 55 nm and 62 nm thick α-In_2Se_3 film. (i) Thickness-dependent curve of coercive field of In_2Se_3 nanosheets.

Figure 4 PFM analysis of α-In_2Se_3 samples exfoliated onto Pt substrate. (a) Topography of a 6 nm α-In_2Se_3 film and (b) the corresponding OOP phase image after writing two square patterns sequentially.

2.3 High-temperature coercive field of the CVD-grown In_2Se_3

Beyond the robust room-temperature ferroelectricity, α-In_2Se_3 layers own a relatively high Curie temperature above 200 °C compared to most of the other 2D vdW ferroelectrics, which further increases when the layer thickness of α-In_2Se_3 is reduced [14, 22, 30-33]. There exists a great potential for 2D α-In_2Se_3 to utilize for nanoelectronic devices working at elevated temperature. In order to study the high-temperature stability of the ferroelectric properties of α-In_2Se_3, PFM equipped with a polyheater was used. Off-field OOP hysteresis loops of the CVD-grown α-In_2Se_3 samples (transferred onto Pt substrates) were recorded at a wide temperature ranging from 25 °C to 200 °C. Fig. 5(a)-(c) illustrates the ferroelectric phase switching loops of 10 nm, 25 nm and 62 nm thick In_2Se_3 films at various temperature, showing clear switching between two polarization states. Furthermore, the temperature-E_c relationship of the In_2Se_3 nanosheets with the different thicknesses is demonstrated by plotting the E_c against temperature in Fig. 5(d)-(f), respectively. There are only minor variations in the E_c of the 10 nm, 25 nm and 62 nm thick In_2Se_3 when the temperature increases, and their ferroelectric characteristics can maintain up to 200 °C. The small increase in the E_c is presumably induced by the clamping effect between the In_2Se_3-substrate interfaces when rising the temperature in the range below 100 °C, and the possible Se defects on the surface of the α-In_2Se_3 samples which are investigated later by Raman spectroscopy [34-36]. OOP phase images of the 25 nm In_2Se_3 nanoflake at different temperature are presented in Fig. S2 in the ESM, where ferroelectric domains can be visualized from 25 °C to 175 °C. When the temperature reached up to 200 °C or above, the conductive AFM probe to perform PFM measurements was not appropriate to work at relatively elevated temperature and the PFM signals were not stable, leading to a great difficulty to conduct PFM measurements above 200 °C. Moreover, the 25 nm In_2Se_3 nanoflake was damaged during the single-switching hysteresis loop measurements at 200 °C, as illustrated in Fig. S3 in the ESM.

On the other hand, the crystal phase of the In_2Se_3 samples after high-temperature PFM characterization was verified with temperature-variable Raman spectroscopy. It is noted that only thicker In_2Se_3 samples were tested because ultrathin samples might easily be destroyed even under the very low laser power (0.05 mW). Figure 5(g) and (h) show the Raman spectra of 16 nm and 62 nm thick In_2Se_3 samples measured at the temperatures up to 235 ºC. There is no observable shifting from 107 cm^{-1} to 110 cm^{-1} of the A_1 (LO+TO) phonon mode, suggesting there is no α → β phase transformation below 235 ºC [30, 31], and the as synthesized In_2Se_3 films with thickness below 62 nm steadily remained in the ferroelectric α-phase below 235 ºC. Besides the Raman shifting of α-In_2Se_3, there is an additional peak found at ~253 cm^{-1} in the 62 nm thick sample corresponding to the vibration mode of Se_8 rings [37], signifying the presence of Se defects in the surface site. Consequently, the characterizations have depicted 2D α-In_2Se_3 with merit in stable ferroelectrics at high temperature.

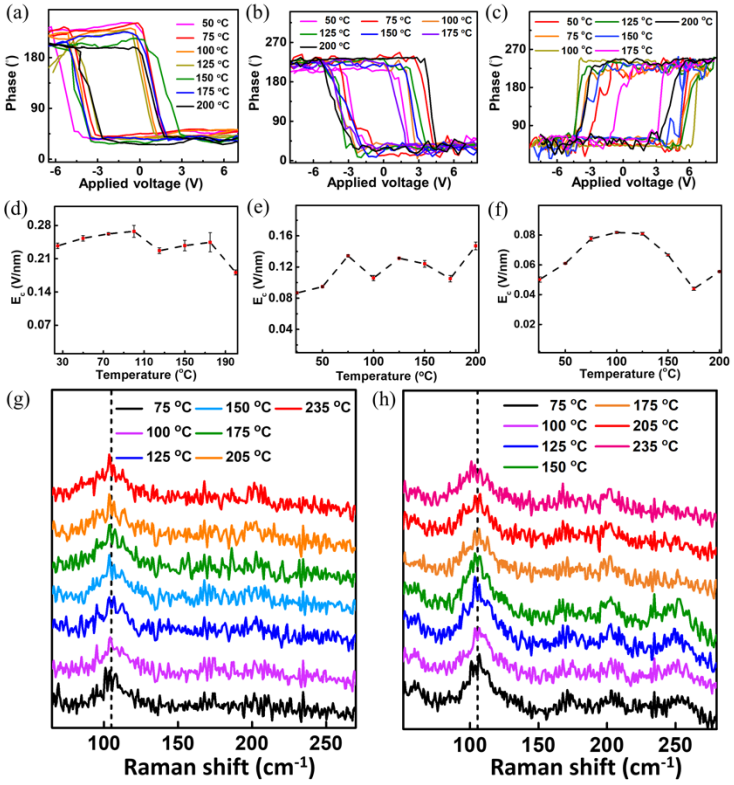

Figure 5 PFM phase hysteresis loops of (a) 10 nm, (b) 25 nm and (c) 62 nm thick CVD-grown In_2Se_3 nanosheets at various temperature, and (d-f) their corresponding temperature-dependent curves of coercive field. Raman spectra of (g) 16 nm and (h) 62 nm In_2Se_3 thin films at various temperature.

As mentioned above, ferroelectric Curie temperature of the prototypical ferroelectric perovskite oxides reduces with a decrease in ferroelectric film thickness. For instance, the critical temperature is 490 ºC for bulk $PbTiO_3$, 120 ºC for $BaTiO_3$ and −270 ºC for $SrTiO_3$ [38-39]. Although the intrinsic transition temperatures of several ferroelectric perovskite oxides are above room temperature, there exists a critical thickness for them to retain ferroelectricity above room temperature which typically around a few to tens of nanometers and is usually thicker than the thickness of monolayer 2D materials [8, 39-41]. When the ferroelectric perovskite oxide films are thinned down to nanoscale, their ferroelectricity diminishes at an even lower temperature, greatly limiting their possibilities to function at a high-temperature environment. In contrast, owing to the merits of the vdW structure, the Curie temperature of 2D vdW ferroelectric materials does not decline with their thickness and is more advantageous to utilize in high-temperature devices. On the other hand, among most of the experimentally confirmed 2D vdW materials exhibiting OOP ferroelectricity, their Curie temperature is usually not much higher than room temperature. The Curie temperature of $CuInP_2S_6$ is at ~42 ºC [42], and that of the $MoTe_2$ and WTe_2 is above room-temperature (about tens of degree Celsius) [15-16]. Although the ferroelectric transition temperature for these materials is above room-temperature, they are not appropriate to use in high-temperature electronic devices which often demand for a higher operating temperature. In comparison, 2D α-In_2Se_3 can maintain stable ferroelectric polarization above 200 ºC down to 10 nm thick as demonstrated in this work, superior to the other 2D vdW ferroelectrics. This is probably due to the interlocking of the OOP and IP polarization in α-In_2Se_3 that effectively stabilizes the ferroelectricity down to monolayer at room-temperature, and the mechanism is different from $CuInP_2S_6$ and other 2D vdW ferroelectrics [19, 22]. Driven by the advantage of a significantly higher Curie temperature, 2D α-In_2Se_3 can be considered as a potential candidate for next-generation nanoscale non-volatile memory devices where good stability at high temperature are required, especially when placed near engines and other electronic components.

3. Conclusion

In summary, we have for the first time studied experimentally the robust OOP ferroelectricity of α-phase In_2Se_3 down to 10 nm from room-temperature to high-temperature. The phase switching behaviors and ferroelectric domains of In_2Se_3 from room-temperature to high-temperature (200 ºC) are demonstrated experimentally via PFM, illustrating its intrinsic high Curie temperature. Moreover, the coercive field for switching the polarization direction rises substantially when the In_2Se_3 films become thinner, and there is no obvious fluctuation in the coercive field with the increase in temperature. Our findings broaden the functionalities of ultrathin In_2Se_3 films and provide essential insights into promising high-temperature nanoelectronic applications based on In_2Se_3 and other 2D materials.

4. Methods

4.1 Sample preparation

The 2D In_2Se_3 nanoflakes were grown on flexible mica substrates through CVD method. Se and In_2O_3 powders were used as the precursors with 10% H_2/Ar mix gas as the carrier gas. The precursors were placed at separate quartz boats and the Se source was placed in the upstream. The Se and In_2O_3 powders were heated to 300 ºC and 660 ºC, respectively, and the temperature was held for 40 min in atmospheric pressure with carrier gas flowing at ~30 sccm. The 2D In_2Se_3 nanoflakes were deposited on the mica substrates placed above the In_2O_3 powders. After the deposition process, the CVD furnace was cooled down naturally to room-temperature. Ultrathin In_2Se_3 nanosheets were also exfoliated from bulk α-In_2Se_3 crystal onto Pt substrate for PFM characterization.

4.2 Transfer of 2D In_2Se_3 nanoflakes

The In_2Se_3 samples were transferred onto specified substrates via polystyrene (PS)-mediated transfer method. A layer of PS was spin-coated onto the surface of the In_2Se_3 nanoflakes at 3000 rpm for 1 min and baked at 150 ºC for 5 min. With the assistance of water, the PS/ In_2Se_3 film was then peeled off from the mica substrate and fished by the target substrate. After the transfer process, the PS layer was dissolved in toluene, leaving the In_2Se_3 samples on the target substrate.

4.3 Raman, AFM, TEM and XPS characterization

The Raman spectra were detected using an excitation laser with 532 nm wavelength and 1 μm spot size (Witec Confocal Raman system). The power of the laser was controlled at 0.2~0.4 mW in order to avoid damage to the samples. The AFM measurement was conducted by Asylum MFP-3D Infinity device under contact mode. TEM sample was prepared by PS-assisted transfer method onto copper grid. The HRTEM image and SAED pattern were acquired using JEOL 2100F Transmission Electron Microscope device with 200 kV accelerating voltage and an exposure time of 0.5 s. The elemental composition of the samples was performed by XPS (Thermo Scientific Nexsa system).

4.4 Ferroelectric measurements

The ferroelectric properties were investigated by PFM using the same commercial device for AFM characterization (Asylum MFP-3D Infinity). A conductive probe (OMCL-AC240TM) was driven at a tip-sample contact resonance frequency of ~300 kHz and an ac bias V_{ac} of 1-2 V was applied. The PFM images, single-point off-field phase and amplitude hysteresis loops were obtained in dual ac resonance tracking piezo force microscopy (DART-PFM) mode. The high-temperature single-point off-field switching hysteresis loops were collected in DART-PFM mode with a polyheater equipped.

Acknowledgements

This research was supported by the grant from Research Grants Council of Hong Kong (GRF No. PolyU 153033/17P).

Electronic Supplementary Material: Supplementary material (AFM image and height profile of α-In_2Se_3, PFM phase images and topographical images of α-In_2Se_3 at different temperature) is available in the online version of this article at http:http://dx.doi.org/10.1007/s12274-***-****-* (automatically inserted by the publisher).

References

[1] Cui, C.; Xue, F.; Hu, W. J.; Li, L. J. Two-dimensional materials with piezoelectric and ferroelectric functionalities. *npj 2D Mater. Appl.* **2018**, *2*, 18.

[2] Zhang, Y.; Jie, W.; Chen, P.; Liu, W.; Hao, J. Ferroelectric and piezoelectric effects on the optical process in advanced materials and devices. *Adv. Mater.* **2018**, *30*, 1707007.

[3] Jeong, D. S.; Thomas, R.; Katiyar, R. S.; Scott, J. F.; Kohlstedt, H.; Petraru, A.; Hwang, C. S. Emerging memories: resistive switching mechanisms and current status. *Rep. Prog. Phys.* **2012**, *75*, 076502.

[4] Zheng, F.; Xin, Y.; Huang, W.; Zhang, J.; Wang, X.; Shen, M.; Dong, W.; Fang, L.; Bai, Y.; Shen, X.; Hao, J. Above 1% efficiency of a ferroelectric solar cell based on the Pb(Zr, Ti)O_3 film. *J. Mater. Chem. A* **2014**, *2*, 1363-1368.

[5] Yang Z.; Hao, J. Recent progress in 2D layered III-VI semiconductors and their heterostructures for optoelectronic device applications. *Adv. Mater. Technol.* **2019**, 1900108.

[6] Yuan, S.; Yang, Z.; Xie, C.; Yan, F.; Dai, J.; Lau, S. P.; Chan, H. L.; Hao, J. Ferroelectric-driven performance enhancement of graphene field-effect transistors based on vertical tunneling heterostructures. *Adv. Mater.* **2016**, *28*, 10048-10054.

[7] Gao, P.; Zhang, Z.; Li, M.; Ishikawa, R.; Feng, B.; Liu, H. J.; Huang, Y. L.; Shibata, N.; Ma, X.; Chen, S. et al. Possible absence of critical thickness and size effect in ultrathin perovskite ferroelectric films. *Nat. Commun.* **2017**, *8*, 15549.

[8] Junquera, J.; Ghosez, P. Critical thickness for ferroelectricity in perovskite ultrathin films. *Nature* **2003**, *422*, 506.

[9] Lee, D.; Lu, H.; Gu, Y.; Choi, S. Y.; Li, S. D.; Ryu, S.; Paudel, T. R.; Song, K.; Mikheev, E.; Lee, S. et al. Emergence of room-temperature ferroelectricity at reduced dimensions. *Science* **2015**, *349*, 1314-1317.

[10] Lang, X. Y. and Jiang, Q. Size and interface effects on curie temperature of perovskite ferroelectric nanosolids. *J. Nanoparticle Res.* **2007**, *9*, 595-603.

[11] Balachandran, P. V.; Xue, D.; Lookman, T. Structure-curie temperature relationships in $BaTiO_3$-based ferroelectric perovskites: anomalous behavior of (Ba, Cd) TiO_3 from DFT, statistical inference, and experiments. *Phys. Rev. B*. **2016**, *93,* 144111.

[12] Chang, K.; Liu, J.; Lin, H.; Wang, N.; Zhao, K.; Zhang, A.; Jin, F.; Zhong, Y.; Hu, X.; Duan, W. et al. Discovery of robust in-plane ferroelectricity in atomic-thick SnTe. *Science* **2016**, *353*, 274-278.

[13] Fei, R.; Kang, W.; Yang, L. Ferroelectricity and phase transitions in monolayer group-IV monochalcogenides. *Phys. Rev. Lett.* **2016**, *117*, 097601.

[14] Liu, F.; You, L.; Seyler, K. L.; Li, X.; Yu, P.; Lin, J.; Wang, X.; Zhou, J.; Wang, H.; He, H. et al. Room-temperature ferroelectricity in $CuInP_2S_6$ ultrathin flakes. *Nat. Commun.* **2016**, *7*, 12357.

[15] Yuan, S.; Luo, X.; Chan, H. L.; Xiao, C.; Dai, Y.; Xie, M.; Hao, J. Room-temperature ferroelectricity in $MoTe_2$ down to the atomic monolayer limit. *Nat. Commun.* **2019**, *10*, 1775.

[16] Fei, Z.; Zhao, W.; Palomaki, T. A.; Sun, B.; Miller, M. K.; Zhao, Z.; Yan, J.; Xu, X.; Cobden, D. H. Ferroelectric switching of a two-dimensional metal. *Nature* **2018**, *560*, 336.

[17] Ding, W.; Zhu, J.; Wang, Z.; Gao, Y.; Xiao, D.; Gu, Y.; Zhang, Z.; Zhu, W. Prediction of intrinsic two-dimensional ferroelectrics in In_2Se_3 and other III_2-VI_3 van der Waals materials. *Nat. Commun.* **2016**, *8*, 14956.

[18] Zhou, Y.; Wu, D.; Zhu, Y.; Cho, Y.; He, Q.; Yang, X.; Herrera, K.; Chu, Z.; Han, Y.; Downer, M. C. et al. Out-of-plane piezoelectricity and ferroelectricity in layered α- In_2Se_3 nanoflakes. *Nano Lett.* **2017**, *17*, 5508-5513.

[19] Cui, C.; Hu, W.; Yan, X.; Addiego, C.; Gao, W.; Wang, Y.; Wang, Z.; Li, L.; Cheng, Y.; Li, P. et al. Intercorrelated in-plane and out-of-plane ferroelectricity in ultrathin two-dimensional layered semiconductor In_2Se_3. *Nano Lett.* **2018**, *18*, 1253-1258.

[20] Poh, S.; Tan, S. J. R.; Wang, H.; Song, P.; Abidi, I. H.; Zhao, X.; Dan, J.; Chen, J.; Lu, Z.; Pennycook, S. J. et al. Molecular-beam epitaxy of two-dimensional In_2Se_3 and its giant electroresistance switching in ferroresistive memory junction. *Nano Lett.* **2018**, *18*, 6340-6346.

[21] Xue, F.; Hu, W.; Lee, K.; Lu, L.; Zhang, J.; Tang, H.; Han, A.; Hsu, W.; Tu, S.; Chang, W. et al. Room-temperature ferroelectricity in hexagonally layered α-In_2Se_3 nanoflakes down to the monolayer limit. *Adv. Funct. Mater*. **2018**, *28*, 1803738.

[22] Xiao, J.; Zhu, H.; Wang, Y.; Feng, W.; Hu, Y.; Dasgupta, A.; Han, Y.; Wang, Y.; Muller, D.; Martin, L. et al. Intrinsic two-dimensional ferroelectricity with dipole locking. *Phys. Rev. Lett.* **2018**, *120*, 227601.

[23] Wan, S.; Li, Y.; Li, W.; Mao, X.; Zhu W.; Zeng, H. Room-temperature ferroelectricity and a switchable diode effect in two-dimensional α-In_2Se_3 thin layers. *Nanoscale* **2018**, *10*, 14885-14892.

[24] Zhou, J.; Zeng, Q.; Lv, D.; Sun, L.; Niu, L.; Fu, W.; Liu, F.; Shen, Z.; Jin, C.; Liu, Z. Controlled synthesis of high-quality monolayered α-In_2Se_3 via physical vapor deposition. *Nano Lett.* **2015**, *15*, 6400-6405.

[25] Wan, S.; Li, Y.; Li, W.; Mao, X.; Wang, C.; Chen, C.; Dong, J.; Nie, A.; Xiang, J.; Liu, Z. et al. Nonvolatile ferroelectric memory effect in ultrathin α-In_2Se_3. *Adv. Funct. Mater.* **2019**, *29*, 1808606.

[26] Küpers, M.; Philipp, K.; Alexander, M.; Joachim, M.; Ulli, E.; Matthias, W.; Richard, D. Controlled crystal growth of indium selenide, In_2Se_3, and the crystal structures of α-In_2Se_3. *Inorg. Chem.* **2018**, *57*, 11775-11781.

[27] Dawber, M.; Chandra, P.; Littlewood, P. B.; Scott, J. F. Depolarization corrections to the coercive field in thin-film ferroelectrics. *J. Phys.: Condens. Matter* **2003**, *15*, L393.

[28] Jo, J. Y.; Kim, Y. S.; Noh, T. W.; Yoon, J. G.; Song, T. K. Coercive fields in ultrathin $BaTiO_3$ capacitors. *Appl. Phys. Lett.* **2006**, *89*, 232909.

[29] Ducharme, S.; Fridkin, V. M.; Bune, A. V.; Palto, S. P.; Blinov, L. M.; Petukhova, N. N.; Yudin, S. G. Intrinsic ferroelectric coercive field. *Phys. Rev. Lett.* **2000**, *84*, 175.

[30] Tao, X.; Gu, Y. Crystalline-crystalline phase transformation in two-dimensional In_2Se_3 thin layers. *Nano Lett.* **2013**, *13*, 3501-3505.

[31] Liu J.; Pantelides, S. Pyroelectric response and temperature-induced α-β phase transitions in α-In_2Se_3 and other α-III_2VI_3 (III= Al, Ga, In; VI= S, Se) monolayers. *2D Mater.* **2018**, *6*, 025001.

[32] Xu, B.; Xiang, H.; Xia, Y.; Jiang, K.; Wan, X.; He, J.; Yin, J.; Liu, Z. Monolayer $AgBiP_2Se_6$: an atomically thin ferroelectric semiconductor with out-plane polarization. *Nanoscale* **2017**, *9*, 8427-8434.

[33] Gerra, G.; Tagantsev, A. K.; Setter, N.; Parlinski, K. Ionic polarizability of conductive metal oxides and critical thickness for ferroelectricity in $BaTiO_3$. *Phys. Rev. Lett.* **2006**, *96*, 107603.

[34] Qiao, H.; He, C.; Wang, Z.; Pang, D.; Li, X.; Liu, Y; Long, X. Influence of Mn dopants on the electrical properties of Pb ($In_{0.5}Nb_{0.5}$) O_3-$PbTiO_3$ ferroelectric single crystals. *RSC Adv.* **2017**, *7*, 32607-32612.

[35] Zhang, X.; Xu, H.; Zhang, Y. Temperature dependence of coercive field and fatigue in poly (vinylidene fluoride-trifluoroethylene) copolymer ultra-thin films. *J. Phys. D: Appl. Phys.* **2011**, *44*, 155501.

[36] Luo, J.; Sun, W.; Zhou, Z.; Bai, Y.; Wang, Z. J.; Tian, G.; Chen, D.; Gao, X.; Zhu, F.; Li, J. F. Domain evolution and piezoelectric response across thermotropic phase boundary in (K, Na) NbO_3-based epitaxial thin films. *ACS Appl. Mater. Interfaces* **2017**, *9*, 13315-13322.

[37] Ho, C. H. Amorphous effect on the advancing of wide-range absorption and structural-phase transition in γ-In_2Se_3 polycrystalline layers. *Sci. Rep.* **2014**, *4*, 4764.

[38] Mbarki, R.; Haskins, J. B.; Kinaci, A.; Cagin, T. Temperature dependence of flexoelectricity in $BaTiO_3$ and $SrTiO_3$ perovskite nanostructures. *Phys. Lett. A* **2014**, *378*, 2181-2183.

[39] Almahmoud, E.; Kornev, I.; Bellaiche, L. Dependence of Curie temperature on the thickness of an ultrathin ferroelectric film. *Phys. Rev. B* **2010**, *81*, 064105.

[40] Fong, D. D.; Stephenson, G. B.; Streiffer, S. K.; Eastman, J. A.; Auciello, O.; Fuoss, P. H.; Thompson, C. Ferroelectricity in ultrathin perovskite films. *Science* **2004**, *304*, 1650-1653.

[41] Ishikawa, K.; Nomura, T.; Okada, N.; Takada, K. Size effect on the phase transition in $PbTiO_3$ fine particles. *Jpn. J. Appl. Phys*. **1996**, *35*, 5196.

[42] Simon, A.; Ravez, J.; Maisonneuve, V.; Payen, C.; Cajipe, V. B. Paraelectric-ferroelectric transition in the lamellar thiophosphate $CuInP_2S_6$. *Chem. Mater.* **1994**, *6*, 1575-1580.